Journal of Orthopaedics 64 (2025) 7–12

Contents lists available at ScienceDirect

Journal of Orthopaedics

journal homepage: www.elsevier.com/locate/jor

Dynamic parallel traction theoretical model for the application and validation in femoral neck fractures - a finite element analysis

Jiarui Li [a,d,1], Kunyue Xing [b,1], Wenzhuo Wang [a,e], Li Sun [a], Linyuan Xue [a], Jiyao Xing [a], Xiaolin Wu [a,*], Dongming Xing [a,c,**]

[a] The Affiliated Hospital of Qingdao University, Qingdao Cancer Institute, Qingdao University, Qingdao, 266071, China
[b] Institute of Health Informatics, Faculty of Population Health Sciences, University College London, London, E14 5AA, United Kingdom
[c] School of Life Sciences, Tsinghua University, Beijing, 100084, China
[d] College of Computer Science and Technology, Qingdao University, Qingdao, 266071, China
[e] College of Electrical Engineering, Qingdao University, Qingdao, 266071, China

ARTICLE INFO

Keywords:
New hypothesis
Dynamic parallel traction
Finite element analysis
Femoral neck fracture

ABSTRACT

Study objective: This study aims to validate the application effects of a novel theoretical model of dynamic parallel traction in the treatment of femoral neck fractures through three-dimensional finite element analysis. By simulating the femoral neck fracture model, we explore the promotional effect of dynamic parallel traction on fracture healing.

Method: A digital 3D femur model was constructed using high-resolution computed tomography data of the lower limbs of a 70-year-old elderly subject. An axial compression of 500N was applied at different traction angles (0°, 10°, 20°, 30°, 40°, 50°). The equivalent stress distribution and deformation of the femur geometric model were calculated at each angle under the six α angles. Statistical analysis was performed using One-Way ANOVA.

Results: At the parallel angle ($\alpha = 0°$), the maximum stress on the entire femur occurred at the trochanteric fossa, with a value of 7.945 MPa ($\alpha = 0°$). The maximum deformation was at the fovea capitis, with a value of 104.13 mm ($\alpha = 0°$). As the traction angle gradually increased ($\alpha = 10°$, $\alpha = 20°$, $\alpha = 30°$, $\alpha = 40°$, $\alpha = 50°$), the maximum stress shifted gradually to the medial cortex of the femoral shaft, with values of 11.236 MPa ($\alpha = 10°$), 15.196 MPa ($\alpha = 20°$), 19.263 MPa ($\alpha = 30°$), 23.149 MPa ($\alpha = 40°$), and 26.311 MPa ($\alpha = 50°$). The maximum deformation remained at the fovea capitis but increased to 131.87 mm ($\alpha = 10°$), 181.96 mm ($\alpha = 20°$), 228.2 mm ($\alpha = 30°$), 271.15 mm ($\alpha = 40°$), and 307.41 mm ($\alpha = 50°$). One-Way ANOVA revealed that traction angle significantly influenced the stress distribution ($F = 4.419$, $p = 0.0022$) and deformation magnitude ($F = 4.023$, $p = 0.0040$) at the proximal femur, indicating that traction angle is a critical factor affecting stress distribution and deformation.

Conclusion: With the increase of the traction angle, the mechanical properties of the proximal femur decrease, indicating an increased risk of non-union and complications. Additionally, the study proves the effectiveness of the "dynamic parallel traction" theory.

1. Introduction

Femoral neck fractures are a common orthopedic issue, accounting for 3.6 % of all fractures in the body and 48 %–54 % of hip fractures.[1,2] They most frequently occur in the elderly,[3] usually as a result of low-energy trauma,[4] such as falls. In contrast, femoral neck fractures in young individuals are typically caused by high-energy violent injuries.[5] Current treatment strategies are generally divided into two categories: surgical treatment,[6-8] and non-surgical treatment.[9] Surgical treatment is often the preferred method due to its shorter treatment duration and better outcomes.[10] However, in areas with limited resources and in elderly patients with surgical contraindications, non-surgical treatment is commonly adopted.[11] Traction therapy,[12] is a common form of non-surgical treatment. Traditional traction methods include bone

* Corresponding author.
** Corresponding author. The Affiliated Hospital of Qingdao University, Qingdao Cancer Institute, Qingdao University, Qingdao, 266071, China.
E-mail addresses: fyqs01@qdu.edu.cn (X. Wu), xdm_tsinghua@163.com (D. Xing).
[1] Co-first Author: Jiarui Li, Kunyue Xing.

https://doi.org/10.1016/j.jor.2024.10.057
Received 25 October 2024; Accepted 31 October 2024
Available online 5 November 2024

traction and skin traction, but these are prone to misalignment of the traction angle,[13] and patient comfort during treatment is low. Modern traction methods include electric traction beds, which provide continuous traction force, and mechanical traction devices, which allow for the adjustment of traction weight. However, none of these methods allow for the adjustment of the traction angle when misalignment occurs.

A review of current research reveals a gap in the dynamic adjustment of traction angles and the maintenance of traction stability. This not only highlights the limitations of existing research but also points to potential new directions for future studies. The aim of this study is to fill these research gaps and further optimize the traction treatment methods for femoral neck fractures. The proposed dynamic parallel traction theoretical model is based on an angle compensation system that can adjust the angle of deviation in space, thereby maintaining a stable state of continuous parallel traction.

The main objectives of this study include: (i) to explore the effect of different traction angles on biomechanical characteristics; (ii) to establish a theoretical model for the dynamic adjustment of traction angles; (iii) to validate the effectiveness of the "dynamic parallel traction" theoretical model. To quantify the spatial configuration of the proximal femur, we defined the angle between the traction angle and the reference axis in the spatial plane as the α angle. Using three-dimensional finite element analysis, we evaluated a series of mechanical indicators, such as stress distribution and total deformation, under different α angles.

2. Materials and method

2.1. Three-dimensional reconstruction and finite element analysis

In this study, we conducted a high-resolution computed tomography (HRCT) scan of the left lower limb of a 70-year-old female subject using a Siemens 64-slice CT scanner to obtain DICOM format image data. These data were processed using MIMICS 17.0 (Materialize, Leuven, Belgium), which involved preprocessing the images, including adjusting the contrast to +20 % and enhancing the brightness to +10 %. Unrelated areas amounting to 20 % were removed using the cropping tool. Within a threshold range of 182–1123 HU, the region growing function was used to fill tissue areas, with a minimum region size set to 10 pixels to exclude noise. During the three-dimensional model construction process, approximately 200 isolated noise points were manually removed, and 5 cavities with a diameter less than 2 mm were filled. The model resolution was set to 0.5 mm, and after three smoothing iterations, the number of faces was reduced to 50 % of the original through the reduction operation. The final model was exported in STL format, consisting of about 150,000 triangular facets.

Subsequently, the model was optimized using GEOMAGIC (3D Systems, Rock Hill, South Carolina, USA) to eliminate defects such as sharp edges, overlapping areas, and cavities. After preprocessing the point cloud data, the "reduce noise" function retained 90 % of the original data information, and the "simplify" function reduced the number of points to 80 % of the original. The "fill holes" function automatically filled cavities larger than 0.2 mm in diameter, ensuring the integrity of the model.

Finally, the model was exported in IGES format, laying the foundation for finite element analysis. A three-dimensional finite element analysis was conducted on the femoral neck, with tetrahedral elements used for meshing. A refined mesh size of 1 mm was applied in the femoral neck region, while a coarser mesh size of 2 mm was used in non-critical areas. The physical and mechanical parameters of the femur included a Young's modulus of 17 GPa, Poisson's ratio of 0.3, density of 1.8 g/cm^3, and yield strength of 100 MPa, with an isotropic material model selected. The model was fixed at the distal end and a physiological load was applied at the proximal end. The load magnitude was set to a 500N axial force, directed perpendicular to the ground, with the point of application at the center of the femoral head (Fig. 1). The analysis mode was static, with an iteration count set to 50, and convergence criteria of displacement convergence tolerance at 1e-5 and force convergence tolerance at 1e-4. The equivalent stress distribution and deformation of the femur were calculated using ANSYS 19.0 (Canonsburg, Pennsylvania, USA).

2.2. Statistical analysis

Data analysis was conducted using GraphPad Prism version 9.5 (GraphPad Software, San Diego, CA, USA). The environmental conditions for all biomechanical experiments were identical. To compare the differences in stress distribution and deformation variables among groups with different traction angles α, we employed one-way ANOVA. In the statistical analysis, we paid particular attention to the p-value and F-value. If the p-value was less than 0.05, the difference between groups was considered statistically significant, indicating a notable difference.

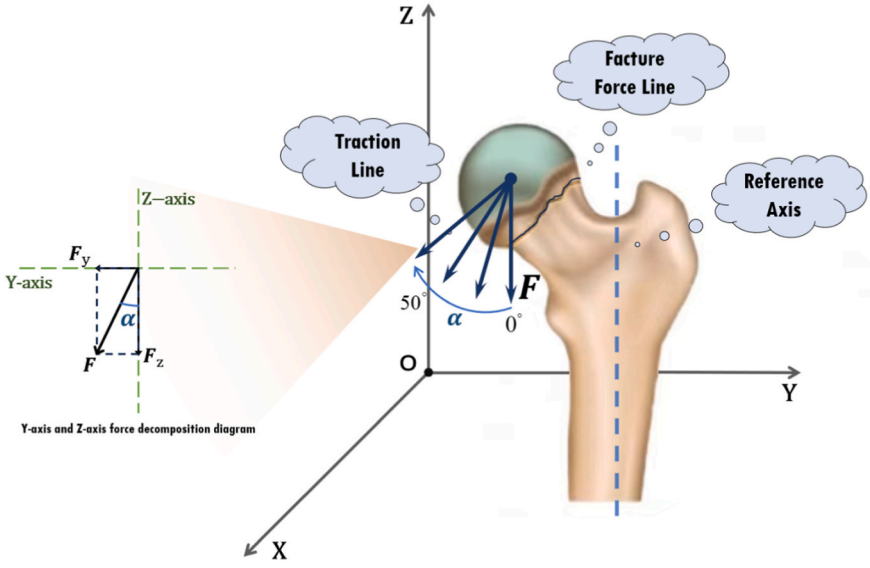

Fig. 1. The point of force application is located at the center of the femoral head, with a 500N axial force applied. The traction angle is defined as the α angle (on the right) relative to the reference axis within the spatial plane. The reference axis is parallel to the z-axis, hence the applied force is decomposed into the z-axis and y-axis (on the left).

2.3. Derivation of the theoretical model for dynamically adjusting traction angles

To achieve dynamic parallel traction and compensate for potential angular offsets during the traction process, we developed an angular compensation system (Fig. 2). The system operates based on geometric relationships and the cosine rule in three-dimensional space. Briefly, our method involves the following steps:

Definition of Traction Force Lines: Define the traction force line L1 under normal conditions and the offset traction force line L1′.

Principle of Angular Compensation: Select a point P on L1' and construct a horizontal plane n and a vertical plane m. Using these two planes, project L1' onto L2 and L3, respectively, and calculate the angles between them.

Geometric Measurement: Select a point Q on L1 and measure the distance d′ between P and Q, as well as the distance d from Q to plane n.

Application of the Cosine Rule: Using the cosine rule to calculate angles and distances, including the distance d'' between point P and the intersection point V of L3, as well as the distances from point W to points V and P, in order to determine the required angle compensation.

Implementation of Angular Compensation: Dynamically adjust the traction force line based on the calculated angles and distances to achieve parallelism with the reference axis.

The detailed derivation of the theoretical model and the calculation steps will be presented in the Results section.

3. Result

3.1. The impact of different traction angles on biomechanical characteristics

Based on the results of the equivalent stress distribution across the entire femur (Fig. 3), under parallel traction ($\alpha = 0°$), the maximum stress occurs at the trochanteric fossa cortex, with a value of 7.945 MPa ($\alpha = 0°$). The maximum deformation is located at the femoral head concavity cortex, with a value of 104.13 mm ($\alpha = 0°$). As the traction angle gradually increases ($\alpha = 10°$, $\alpha = 20°$, $\alpha = 30°$, $\alpha = 40°$, $\alpha = 50°$), the maximum stress progressively shifts to the medial cortex of the femoral shaft, with values of 11.236 MPa ($\alpha = 10°$), 15.196 MPa ($\alpha = 20°$), 19.263 MPa ($\alpha = 30°$), 23.149 MPa ($\alpha = 40°$), and 26.311 MPa ($\alpha = 50°$). The maximum deformation remains at the femoral head concavity cortex but increases to 131.87 mm ($\alpha = 10°$), 181.96 mm ($\alpha = 20°$), 228.2 mm ($\alpha = 30°$), 271.15 mm ($\alpha = 40°$), and 307.41 mm ($\alpha = 50°$). With the increase of the traction angle, the stress distributed in the proximal femoral region, including the medial cortex of the femoral neck, the greater trochanter cortex, and the shaft cortex, all increase (Fig. 3). Among these, the shaft cortex shows the greatest increase in stress. At a traction angle of $\alpha = 50°$, the corresponding maximum stress increases by 2.76 times compared to $\alpha = 0°$ (10.193 MPa). One-way ANOVA ($F = 4.419$, $p = 0.0022$) confirmed the significant differences in equivalent stress distribution under different traction angles, indicating that the traction angle has a significant impact on the stress distribution in the proximal femur (Fig. 5). Simultaneously, the deformation distributed in the proximal femoral region, including the medial cortex of the femoral neck, the greater trochanter cortex, and the femoral head cortex, also increases, with respective increases of 2.95 times (medial femoral neck cortex), 2.95 times (inter-trochanteric cortex), and 2.95 times (femoral head cortex) (Fig. 4). The inter-trochanteric cortex experiences the greatest increase in deformation (112.928 mm). One-way ANOVA ($F = 4.023$, $p = 0.0040$) also confirmed the significant differences in deformation under different traction angles, suggesting that an increase in traction angle leads to a significant increase in deformation (Fig. 6).

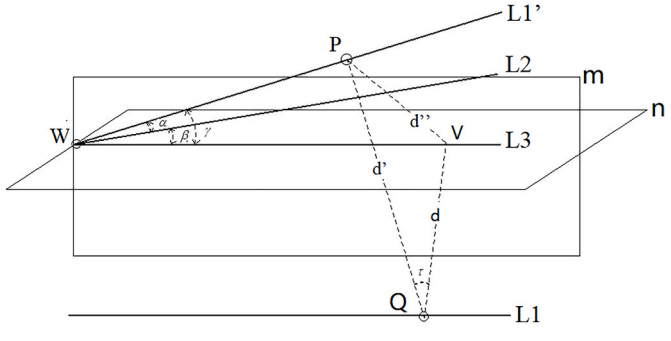

Fig. 2. Schematic Diagram of the Dynamic Parallel Traction Angular Compensation System. L1 represents the traction force line under normal conditions, and L1' represents the traction force line after offset. n denotes the horizontal plane, m denotes the vertical plane, L2 and L3 represent the lines where L1' is projected onto planes m and n, respectively. W is the intersection point between L1', L2, and L3. P is a point on L1', Q is a point on L1, and V is a point on L3. d is the distance between Q and V, d' is the distance between P and Q, d'' is the distance between P and V. τ is the angle between QP and QV, α is the angle between L2 and L1', β is the angle between L3 and L2, and γ is the angle between L1' and L3.

3.2. Derivation of the theoretical model for dynamically adjusting traction angles

In the event of angular deviation during traction, the dynamic parallel traction system will adjust the angle in three-dimensional space through the angular compensation system (Fig. 2). The principle of the angular compensation system is as follows:

First, define L1 as the traction force line under normal conditions, and L1' as the traction force line after deviation. Then, select point P on L1', and draw a horizontal plane n parallel to L1 through P, and a plane m perpendicular to plane n. Next, project L1 onto plane m to obtain L2 on plane m, where the angle between L2 and L1' is denoted as α. Subsequently, project line L2 onto plane n to obtain L3 on plane n, where the angle between L3 and L2 is denoted as β. The angle between L1' and L3 is denoted as γ. We need to solve for α and β to compensate for these angles in the respective directions.

The specific steps for the solution are as follows: Select point Q on L1, and measure the distance between points P and Q, denoted as d'. Measure the distance from point Q to plane n, denoted as d, where the angle between d and d' is denoted as τ. The distance from the perpendicular line from point P to point Q intersecting L3 is d'', and using the cosine rule, we have $d^2 + d'^2 - d''^2 = 2dd' \cos\tau$ from which we can solve for d''. Let the intersection point of L1', L2, and L3 be point W. Using the distances dwv (from W to V), dwp (from W to P), and d'', we can solve for γ. According to the cosine rule $d_{wv}{}^2 + d_{wp}{}^2 - d''^2 = 2d_{wv}d_{wp}\cos\gamma$ from which we can solve for γ. Using the three-cosine rule, $\cos\gamma = \cos\alpha\cdot\cos\beta$, we have $\cos\alpha$ and $\cos\beta$, from which we can determine the product of $\cos\alpha$ and $\cos\beta$. Measure the distance from point P to plane m. Since L2 is the projection of L1' onto plane m, the perpendicular foot from L1' to plane m will fall on L2; denote the foot as point X. Measure d_{px} (from P to X) and d_{wx} (from W to X). In Δpwx, using $\tan\alpha = \frac{d_{px}}{d_{wx}}$ and $\alpha = \arctan\frac{d_{px}}{d_{wx}}$, we can solve for α. Also, using $\beta = \arccos\frac{\cos\gamma}{\cos\alpha}$, we can solve for β.

By compensating for the angles α and β, we can once again achieve parallelism between the traction force line and the reference axis.

4. Discussion

4.1. The relationship between non-union rates of fractures and traction angles

In this study, we analyzed the stress distribution characteristics and deformation variables under different traction angles using three-

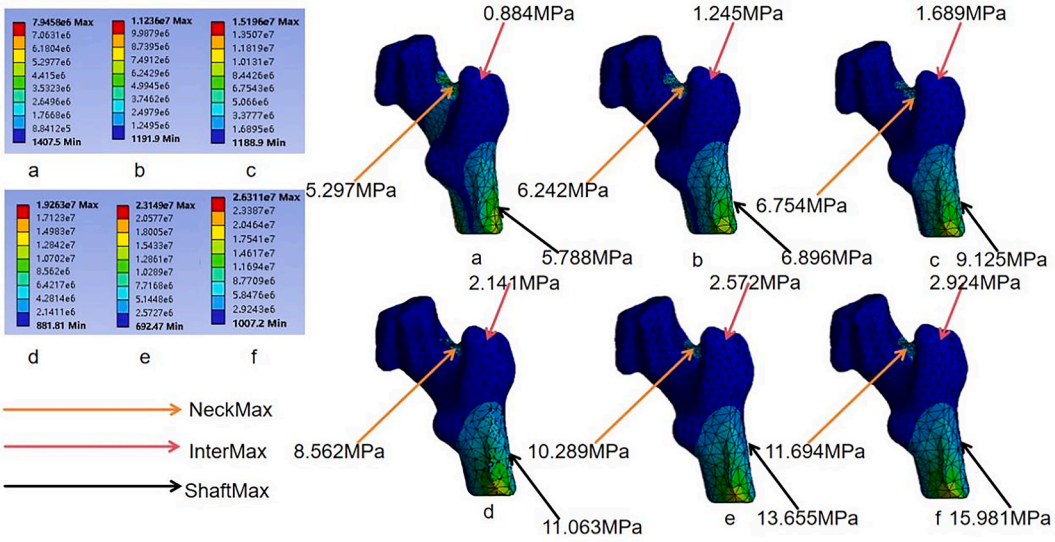

Fig. 3. The equivalent stress distribution of the entire femur under a 500N vertical load at α angles of 0° (a), 10° (b), 20° (c), 30° (d), 40° (e), and 50° (f). The local maximum stresses at the medial femoral neck wall (NeckMax), inter-trochanteric wall (InterMax), and femoral shaft wall (ShaftMax) are indicated in the figure.

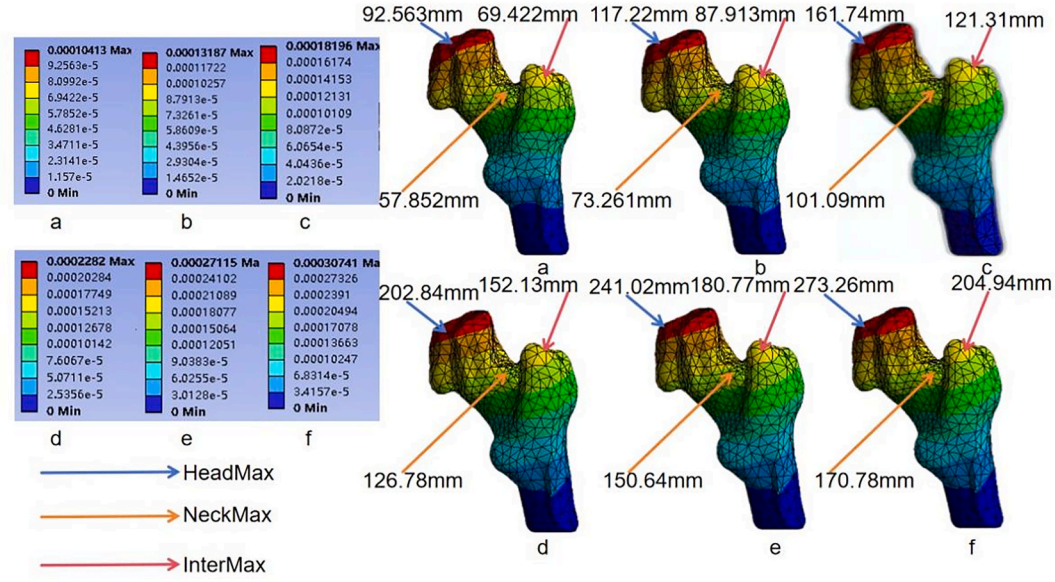

Fig. 4. The deformation of the entire femur under a 500N vertical load at α angles of 0° (a), 10° (b), 20° (c), 30° (d), 40° (e), and 50° (f). The local maximum deformations at the femoral head wall (HeadMax), medial femoral neck wall (NeckMax), and inter-trochanteric wall (InterMax) are indicated in the figure.

dimensional finite element methods. The results revealed that as the traction angle increased, the maximum stress distribution shifted gradually from the trochanteric fossa cortex to the inferior-medial cortex of the femoral shaft, with the maximum stress value increasing from 7.945 MPa to 26.311 MPa. This stress shift may be due to the change in the relative position of the traction force line to the femur, leading to an uneven distribution of the mechanical load borne by the femur.[14] Although the maximum deformation still occurred at the concave side of the femoral head cortex, the value increased from 104.13 mm to 307.41 mm. A one-way analysis of variance confirmed the significant relationship between different traction angles and stress distribution and deformation variables. The correct traction angle is conducive to the alignment and stability of the fracture ends, thereby promoting callus formation. If the traction angle is misaligned, it may lead to instability at the fracture site,[15] prolong healing time,[16] and even increase the risk of non-union or result in malunion.[17] The uneven distribution of mechanical loads on the femur may cause soft tissue damage,[18] compress or injure surrounding blood vessels and nerves, leading to local complications as well as cardiovascular and cerebrovascular damage.[19]

4.2. The clinical significance of the dynamic parallel traction theoretical model

In this study, we propose a theoretical model of "Dynamic Parallel Traction," which is based on an angular compensation system to achieve dynamic adjustment of spatial angular displacement. This model enables the realignment of misaligned angles to maintain a state of parallel traction. The aforementioned three-dimensional finite element analysis demonstrated the advantages of parallel traction over other angular traction methods, thereby validating the effectiveness of our "Dynamic Parallel Traction" theoretical model. Current clinical traction methods, including electric traction beds and mechanical traction devices, can provide continuous traction force, but they do not dynamically adjust for traction misalignment, which can lead to issues with fracture non-

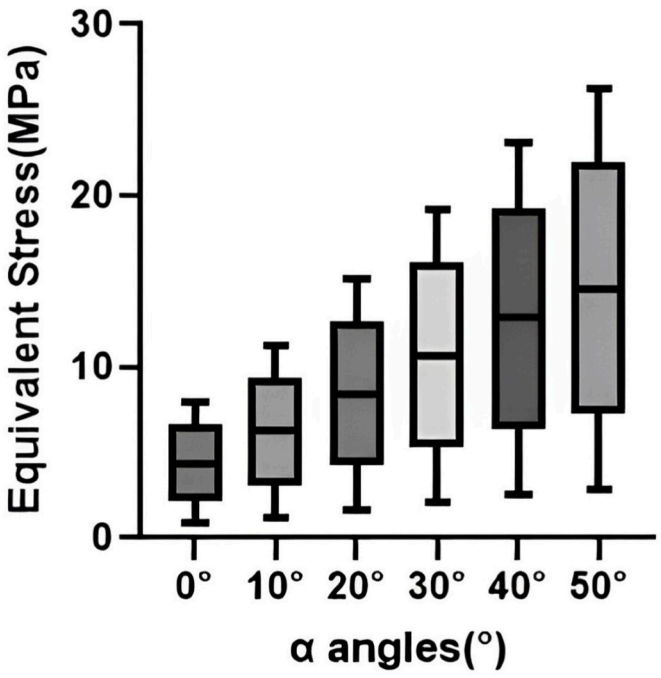

Fig. 5. One-way analysis of variance for the distribution of equivalent stress.

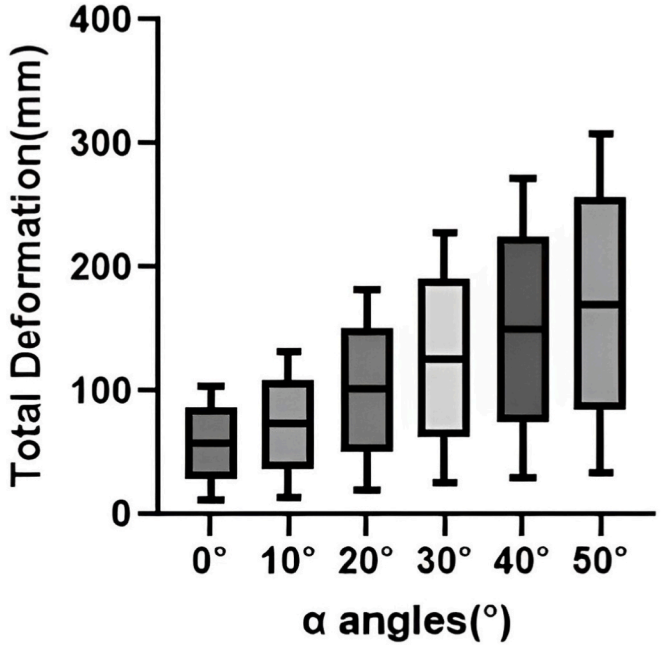

Fig. 6. One-way analysis of variance for the total deformation.

union and affect patient recovery. Our "Dynamic Parallel Traction" theory offers a new perspective for the development of novel traction medical equipment. We have already completed the prototyping of the "Dynamic Parallel Traction" theoretical model (Fig. 7), and it will be subsequently introduced into clinical settings for validation.

4.3. Advantages and disadvantages

This study proposes a novel theoretical model called "Dynamic Parallel Traction," and validates the theory through three-dimensional finite element analysis by examining the distribution of equivalent stress and changes in deformation at different traction angles. This provides a new perspective for the development of novel medical devices. However, there are some limitations in the research process. The representativeness of the samples in this study is insufficient. We conducted high-resolution computed tomography (HRCT) scans on the left lower limb of a 70-year-old elderly patient using a Siemens 64-slice CT scanner to obtain DICOM format image data for three-dimensional finite element analysis, which lacks representativeness. On one hand, the sample size is small; on the other hand, the age representation of the sample is also insufficient. Additionally, we have only theoretically derived the "Dynamic Parallel Traction" model and have not conducted a simulation to verify its dynamic parallel adjustment process. The three-dimensional finite element analysis only studied the advantages of parallel traction compared to other traction angles, without considering the influence of other factors such as traction speed and weight. Moreover, the experiment was conducted under static load conditions, while actual physiological conditions are usually dynamic, which may affect the accuracy of the results. Although our "Dynamic Parallel Traction" model has certain theoretical innovation, its clinical validation will still be a complex issue and requires more in-depth research and exploration in the future.

5. Conclusion

This study validated the effectiveness of the dynamic parallel traction theory model in the treatment of femoral neck fractures through three-dimensional finite element analysis. The research findings indicate that with an increase in traction angle, there is an increase in stress concentration and deformation at the proximal femur, which may lead to an elevated risk of fracture healing complications. The dynamic parallel traction model, by real-time adjustment of the traction angle and compensation for angular offsets, is able to achieve the effect of parallel traction. This method provides a new perspective for the development of related novel medical devices.

CRediT authorship contribution statement

Jiarui Li: Study design, data analysis, manuscript writing. **Kunyue Xing:** Study design, data collection, manuscript contribution. **Wenzhuo Wang:** Data analysis, result interpretation. **Li Sun:** Data collection, study discussion. **Linyuan Xue:** Study design, technical support for data analysis. **Jiyao Xing:** Data collection and preprocessing. **Xiaolin Wu:** Study conception, research supervision, manuscript revision. **Dongming Xing:** Study conception, Funding acquisition, research supervision, manuscript revision.

Guardian/patient's consent

This study has obtained informed consent for experimentation with human subjects. The privacy rights of human subjects must always be respected.

Ethical statement

This study adheres to the Helsinki Declaration of the World Medical Association (WMA) – Ethical Principles for Medical Research Involving Human Subjects.

Declaration of generative AI and AI-assisted technologies in the writing process

During the preparation of this work the authors used ChatGLM in order to polish and improve the expression of the article. After using this tool/service, the authors reviewed and edited the content as needed and take full responsibility for the content of the publication.

Fig. 7. Prototype of the "Dynamic Parallel Traction" Theory (a) Represents the position for the patient's lower limb placement. (b) Represents the lower part of the prototype machine. (c) Represents the angle compensation system. The system is equipped with an internal algorithm for angle compensation that can automatically adjust for angular offsets.

Funding statement

This study was supported by Nature Science Foundation of Shandong Province (ZR2022MH218; ZR20220C165), The Affiliated Hospital of Qingdao University Clinical Medicine + X Research Project (QDFY + X2023141; QDFY + X202101054).

Acknowledgements

We thank all the authors of the manuscript.

References

1. Florschutz AV, Langford JR, Haidukewych GJ, et al. Femoral neck fractures: current management. *J Orthop Trauma*. 2015;29(3):121–129.
2. Jain AK, Mukunth R, Srivastava A. Treatment of neglected femoral neck fracture. *Indian J Orthop*. 2015;49:17–27.
3. Okike K, Hasegawa IG. Current trends in the evaluation and management of nondisplaced femoral neck fractures in the elderly. *JAAOS-Journal of the American Academy of Orthopaedic Surgeons*. 2021;29(4):e154–e164.
4. Reito A, Kuoppala M, Pajulammi H, et al. Mortality and comorbidity after non-operatively managed, low-energy pelvic fracture in patients over age 70: a comparison with an age-matched femoral neck fracture cohort and general population. *BMC Geriatr*. 2019;19:1–7.
5. Gao YS, Zhu ZH, Zhang CQ. Simultaneous bilateral fractures of the femoral neck caused by high energy: a case report and literature review. *Chin J Traumatol*. 2015; 18(5):304–306.
6. Lutnick E, Kang J, Freccero DM. Surgical treatment of femoral neck fractures: a brief review. *Geriatrics*. 2020;5(2):22.
7. Zelle BA, Salazar LM, Howard SL, et al. Surgical treatment options for femoral neck fractures in the elderly. *Int Orthop*. 2022;46(5):1111–1122.
8. Sadeghpour A, Mahdipour S, Sales JG, et al. Non-cannulated versus cannulated cancellous screws for the internal fixation of femoral neck fractures in osteoporotic patients: a single-blind randomized clinical trial. *J Orthop*. 2024;51:32–38.
9. Rutenberg TF, Assaly A, Vitenberg M, et al. Outcome of non-surgical treatment of proximal femur fractures in the fragile elderly population. *Injury*. 2019;50(7): 1347–1352.
10. Ye CY, Liu A, Xu MY, et al. Arthroplasty versus internal fixation for displaced intracapsular femoral neck fracture in the elderly: systematic review and meta-analysis of short-and long-term effectiveness. *Chinese Med J*. 2016;129(21): 2630–2638.
11. Lau BC, Wu HH, Mustafa M, et al. Developing research to change policy: design of a multicenter cost-effectiveness analysis comparing intramedullary nailing to skeletal traction in Malawi. *J Orthop Trauma*. 2018;32:S52–S57.
12. Mustafa Diab M, Shearer DW, Kahn JG, et al. The cost of intramedullary nailing versus skeletal traction for treatment of femoral shaft fractures in Malawi: a prospective economic analysis. *World J Surg*. 2019;43:87–95.
13. Vergano LB, Coviello G, Monesi M. Rotational malalignment in femoral nailing: prevention, diagnosis and surgical correction. *Acta Biomed: Atenei Parmensis*. 2020; 91(suppl 14).
14. Zhang H, Xu X, Wu S, et al. A finite element analysis study based on valgus impacted femoral neck fracture under diverse stances. *Comput Methods Biomech Biomed Eng*. 2022;25(5):475–486.
15. Samsami S, Augat P, Rouhi G. Stability of femoral neck fracture fixation: a finite element analysis. *Proc IME H J Eng Med*. 2019;233(9):892–900.
16. Şahin E, Songür M, Kalem M, et al. Traction table versus manual traction in the intramedullary nailing of unstable intertrochanteric fractures: a prospective randomized trial. *Injury*. 2016;47(7):1547–1554.
17. Xu DF, Bi FG, Ma CY, et al. A systematic review of undisplaced femoral neck fracture treatments for patients over 65 years of age, with a focus on union rates and avascular necrosis. *J Orthop Surg Res*. 2017;12:1–12.
18. Tarchichi J, Daher M, Ghoul A, et al. Pre-operative traction in femoral fractures for pain management: a meta-analysis of comparative studies. *The Archives of Bone and Joint Surgery*. 2024;12(10):683–689.
19. Birch R, Miller J, Surina J, et al. Rate of skin and nerve complications as a result of cutaneous traction with modern foam boots. *Injury*. 2024 Aug;55(8), 111687. https://doi.org/10.1016/j.injury.2024.111687. Epub 2024 Jun 19. PMID: 38954994.